Proteasomal degradation of retinoid X receptor α reprograms transcriptional activity of PPARγ in obese mice and humans

Bruno Lefebvre,[1,2,3,4] Yacir Benomar,[1,2,3,4] Aurore Guédin,[1,2,3,4] Audrey Langlois,[1,2,3,4] Nathalie Hennuyer,[1,2,3,4] Julie Dumont,[1,2,3,4] Emmanuel Bouchaert,[1,2,3,4] Catherine Dacquet,[5] Luc Pénicaud,[6] Louis Casteilla,[6] Francois Pattou,[7] Alain Ktorza,[5] Bart Staels,[1,2,3,4] and Philippe Lefebvre[1,2,3,4]

[1]Univ Lille Nord de France, Lille, France. [2]INSERM, UMR1011, Lille, France. [3]UDSL, Lille, France. [4]Institut Pasteur de Lille, Lille, France. [5]Division of Metabolic Diseases, Institut de Recherches Servier, Suresnes, France. [6]Université de Toulouse, UPS, UMR 5241, Toulouse, France. [7]INSERM U859, Faculté de Médecine de Lille-Pôle Recherche, Lille, France.

Obese patients have chronic, low-grade inflammation that predisposes to type 2 diabetes and results, in part, from dysregulated visceral white adipose tissue (WAT) functions. The specific signaling pathways underlying WAT dysregulation, however, remain unclear. Here we report that the PPARγ signaling pathway operates differently in the visceral WAT of lean and obese mice. PPARγ in visceral, but not subcutaneous, WAT from obese mice displayed increased sensitivity to activation by its agonist rosiglitazone. This increased sensitivity correlated with increased expression of the gene encoding the ubiquitin hydrolase/ligase ubiquitin carboxyterminal esterase L1 (UCH-L1) and with increased degradation of the PPARγ heterodimerization partner retinoid X receptor α (RXRα), but not RXRβ, in visceral WAT from obese humans and mice. Interestingly, increased UCH-L1 expression and RXRα proteasomal degradation was induced in vitro by conditions mimicking hypoxia, a condition that occurs in obese visceral WAT. Finally, PPARγ-RXRβ heterodimers, but not PPARγ-RXRα complexes, were able to efficiently dismiss the transcriptional corepressor silencing mediator for retinoid and thyroid hormone receptors (SMRT) upon agonist binding. Increasing the RXRα/RXRβ ratio resulted in increased PPARγ responsiveness following agonist stimulation. Thus, the selective proteasomal degradation of RXRα initiated by UCH-L1 upregulation modulates the relative affinity of PPARγ heterodimers for SMRT and their responsiveness to PPARγ agonists, ultimately activating the PPARγ-controlled gene network in visceral WAT of obese animals and humans.

Introduction

From a clinical perspective, visceral obesity predisposes to an increased incidence of type 2 diabetes mellitus (T2DM) and associated cardiovascular diseases (1, 2). The visceral white adipose tissue (visWAT; i.e., epididymal WAT) depot is believed to contribute to the low-grade, chronic inflammatory state that occurs in obese patients and animals and favors the progression toward T2DM. This feature stems from the specific functional properties of adipocytes from this WAT depot, which are highly sensitive to β-adrenergic stimulation and relatively resistant to the antilipolytic effects of insulin compared with subcutaneous adipocytes (3). Indeed, although subcutaneous WAT (scWAT; i.e., inguinal WAT) is predominantly, but not exclusively, a lipid storage tissue exhibiting a high adipocyte plasticity, visWAT also triggers complex endocrine regulations by releasing FFAs, hormones, and cytokines that reach the liver through the portal vein (reviewed in ref. 4). How visWAT functions are affected upon disease progression is unknown, but metabolic challenges increase the release of proinflammatory cytokines and decrease that of insulin-sensitizing adipokines by visWAT.

Results from recent clinical trials (ADOPT, DREAM, and PROACTIVE; ref. 5) indicate that the insulin-sensitizing thiazolidinediones (TZDs) are highly efficient in maintaining glycemic control, and may exert pancreas-sparing and vascular-protective effects in T2DM patients. TZDs are synthetic agonists for PPARγ (also known as NR1C3), a member of the nuclear receptor (NR) superfamily. PPARγ is a key regulator of adipocyte differentiation and lipid storage, thereby exerting major effects on energy homeostasis (6). Gene ablation studies have confirmed the major role of adipocyte PPARγ (adPPARγ) in mediating the insulin-sensitizing effect of TZDs in obese mice (7–12). Ligand-activated adPPARγ has a positive effect on glucose homeostasis by favoring scWAT expansion and FFA redistribution to this fat depot (13). Removing FFA from other tissues, including skeletal muscle and visWAT, prevents the so-called lipotoxic effect, which causes insulin resistance and hence translates into a greater insulin sensitivity. TZDs also act directly on visWAT functions by regulating the expression of adipokines (14) and several key metabolic genes (15). Quite intriguingly, however, TZDs exert neither detectable insulin-sensitizing effects nor significant metabolic effects in lean individuals and mice, which suggests that the PPARγ pathway operates differently in normal and pathological conditions (16–18).

PPARγ activates target gene transcription by forming obligate heterodimers with the retinoid X receptor (RXR) isotypes — RXRα, RXRβ, and RXRγ — onto PPAR-responsive elements (PPREs). PPREs are found in genes controlling key steps in lipid and glucose metabolism, such as the adipose-specific fatty acid

Authorship note: Bruno Lefebvre and Yacir Benomar contributed equally to this work.

Conflict of interest: The authors have declared that no conflict of interest exists.

Citation for this article: *J Clin Invest.* 2010;120(5):1454–1468. doi:10.1172/JCI38606.

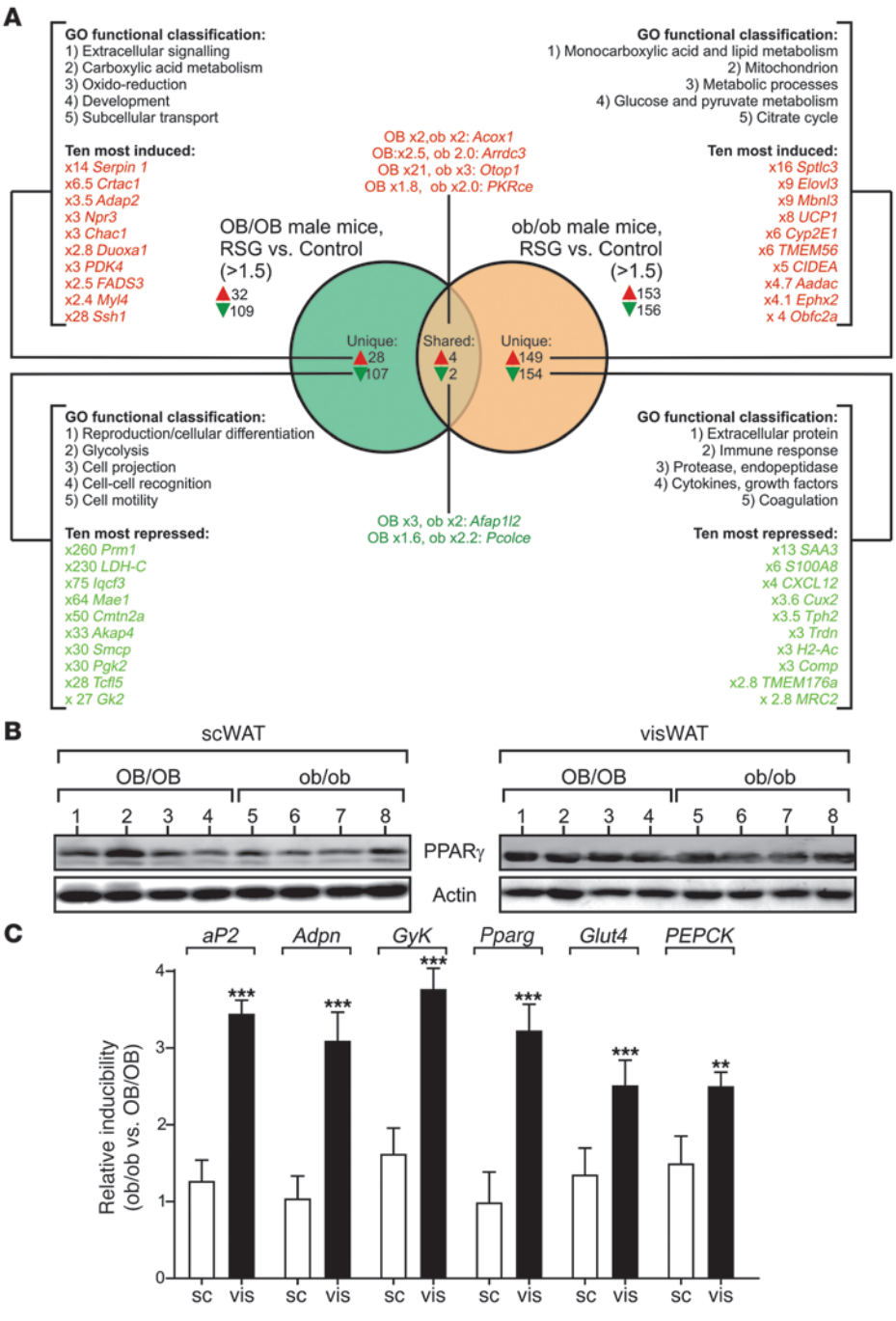

Figure 1

Obese insulin-resistant but not lean mice respond to RSG treatment. Male OB/OB and ob/ob mice were fed a chow diet supplemented or not (control) with RSG corresponding to a 3-mg/kg/d dose. (**A**) Comparative gene expression profiles in OB/OB and ob/ob visWAT treated or not with RSG. 3 samples from each group were analyzed on Affymetrix microarrays and interpreted using the Agilent Genespring GX software. These analysis are summarized here, showing the 10 most upregulated (red) and repressed (green) genes after the 21-day RSG treatment. The 5 most statistically significant Gene Ontology categories are indicated for each subset of genes. (**B**) PPARγ is expressed in scWAT and visWAT. Total proteins were extracted from scWAT and visWAT. Proteins (100 g) were analyzed by reducing SDS-PAGE and Western blotting using anti-PPARγ and anti-β actin antibodies. (**C**) PPARγ target genes display enhanced responsiveness to RSG selectively in visWAT from ob/ob mice. scWAT and visWAT depots were removed from OB/OB, ob/ob, treated OB/OB, and treated ob/ob mice. RNAs were extracted and analyzed for their content in mRNA coding for aP2, Adpn, GyK, Pparγ, Glut4, and PEPCK by RT-QPCR. Fold inductions by RSG were calculated for each condition and are expressed as the ratio of the induction rate measured in ob/ob WAT depots to that measured in OB/OB WAT depots. Data represent mean ± SEM. $^{**}P < 0.01$, $^{***}P < 0.005$.

binding protein (*aP2*), phosphoenolpyruvate carboxykinase (*PEPCK*), or lipoprotein lipase (*LPL*). Of note, RXRα also plays a critical role in adipogenesis in vivo (19). Agonist-mediated activation of PPARγ induces structural transitions occurring in the ligand-binding domain (LBD) of this receptor, creating a hydrophobic groove and a charge clamp that binds LXXLL motifs found in most coactivators, such as the p160-related coactivator family (SRC1–SRC3; ref. 20), the integrator complex CBP/p300 (21), components of the mediator complex (22), and the metabolically regulated coactivator PGC-1α (23, 24). Agonist-dependent coactivator recruitment to PPARγ is concomitant to corepressor dismissal, and both the NR corepressor (NCoR) and the silencing mediator for retinoid and thyroid hormone receptors (SMRT) have been shown to affect PPARγ-controlled cellular processes in distinct cellular backgrounds (25–27).

PPARγ transcriptional activity is therefore dependent on its sequential association with multiprotein complexes. It is thus likely that processes controlling protein stability and degradation also influence the overall activity of the PPARγ complex and may possibly affect its function under conditions of obesity and T2DM. Indeed, components of the ubiquitin-proteasome system (UPS) have been shown to be involved in PPARγ-mediated transactivation (28). Although a few studies documented dysregulated expression of several UPS components in cardiovascular diseases

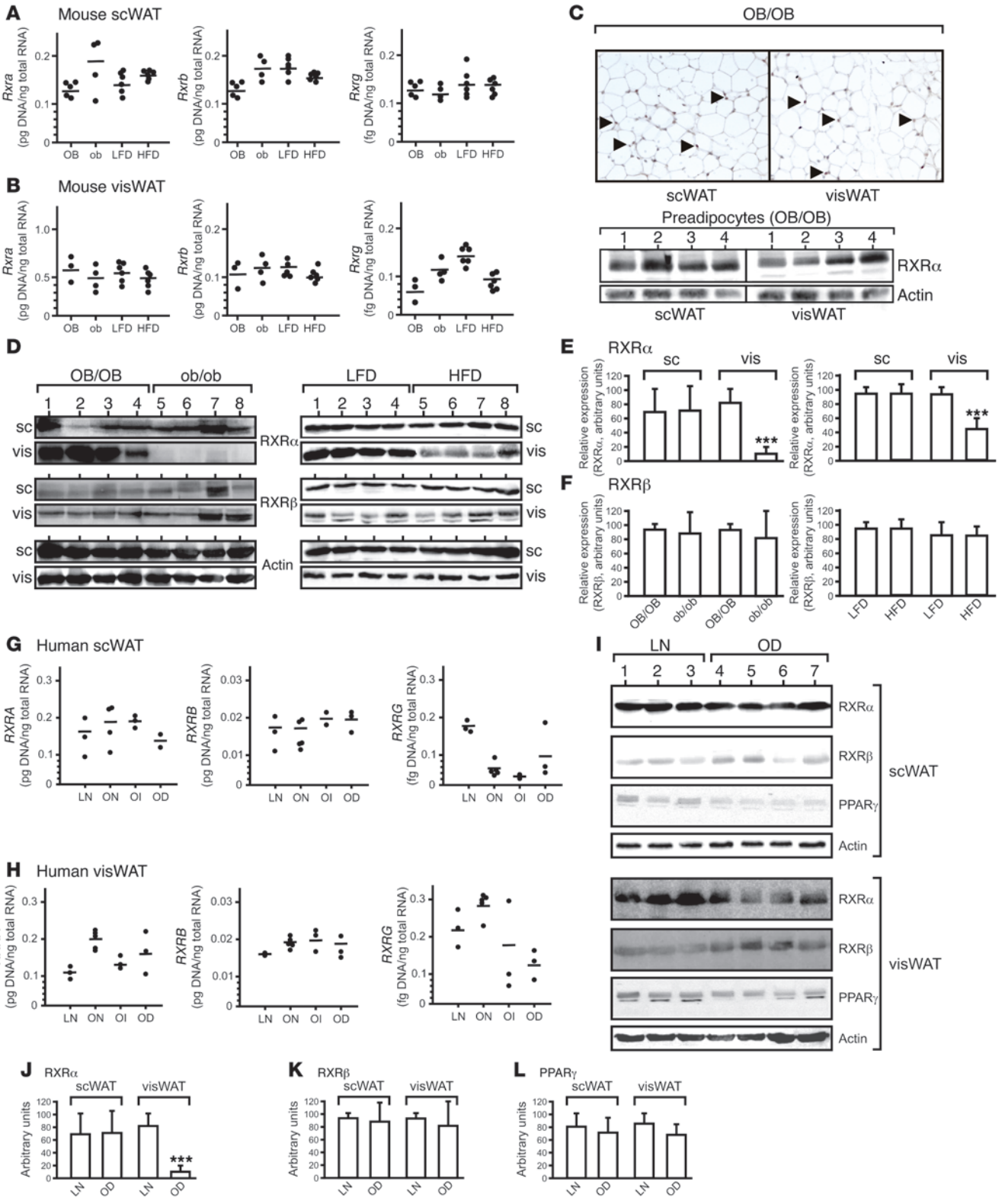
A
Mouse scWAT
Rxra (pg DNA/ng total RNA)
Rxrb (pg DNA/ng total RNA)
Rxrg (fg DNA/ng total RNA)
OB ob LFD HFD
B
Mouse visWAT
C
OB/OB
scWAT
visWAT
Preadipocytes (OB/OB)
RXRα
Actin
D
OB/OB
ob/ob
LFD
HFD
sc
vis
RXRα
RXRβ
Actin
E
RXRα
Relative expression (RXRα, arbitrary units)
***
F
RXRβ
Relative expression (RXRβ, arbitrary units)
OB/OB
ob/ob
LFD
HFD
G
Human scWAT
RXRA (pg DNA/ng total RNA)
RXRB (pg DNA/ng total RNA)
RXRG (fg DNA/ng total RNA)
LN ON OI OD
H
Human visWAT
I
LN
OD
RXRα
RXRβ
PPARγ
Actin
scWAT
visWAT
J
RXRα
K
RXRβ
L
PPARγ
Arbitrary units

Figure 2
RXRα protein, but not mRNA, expression is downregulated in visWAT from obese mice and from obese diabetic patients. (**A** and **B**) RXR mRNA steady-state levels in mouse WAT. mRNAs from scWAT or visWAT were extracted, and *Rxra*, *Rxrb*, and *Rxrg* cDNAs were quantified by QPCR. (**C**) RXRα protein (arrowheads) in WAT sections. Original magnification, ×10. (**D**) RXRα protein in mouse WAT. visWAT and scWAT from OB/OB mice, C57BL/6 mice fed LFD or HFD, or ob/ob mice were probed for their content in RXRα and RXRβ by Western blot analysis. (**E** and **F**) Quantification of data in **D**. The intensity of each RXR band was normalized to actin. The first sample was arbitrarily set to 100%, and each sample was quantified relative to sample 1. Data represent mean ± SEM. ***$P < 0.005$. (**G** and **H**) *RXR* mRNA steady-state levels in human WAT. mRNAs from scWAT and visWAT were analyzed as in **A**. LN, lean normoglycemic; ON, obese normoglycemic; OI, obese glucose intolerant; OD, obese diabetic. (**I**) RXRα, RXRβ, and PPARγ protein levels in human scWAT and visWAT. visWAT from lean or obese diabetic patients was probed for their RXRα, RXRβ, and PPARγ content by Western blot analysis. (**J**–**L**) Quantification of data in **I**. The intensity of each RXR or PPARγ band was normalized to β-actin. The first sample was arbitrarily set to 100%, and each sample was quantified relative to sample 1. Data represent mean ± SEM. ***$P < 0.005$.

(29, 30), a potential contribution of the UPS in the pathogenesis of T2DM and obesity remains unexplored. In the present study, we investigated the relationship among metabolic states, UPS component expression, and the PPARγ signaling pathway. We report that the expression of the ubiquitin hydrolase/ligase ubiquitin carboxyterminal esterase L1 (*UCH-L1*) was specifically and strongly upregulated in visWAT from obese patients and mice. Mimicking hypoxia in vitro also upregulated UCH-L1 expression. This enzyme promotes the selective breakdown of RXRα, which correlates with an increased response of PPARγ to a synthetic agonist in vivo. Moreover, decreasing the RXRα/RXRβ ratio in vitro increased PPARγ transcriptional activity. The molecular basis of this phenomenon was found to be a stable, ligand-insensitive tethering of SMRT to PPARγ-RXRα heterodimers.

Results

PPARγ target genes are more sensitive to agonist stimulation in visWAT of obese mice, but not of lean mice. Because previous studies reported an unexpected insensitivity of lean mice or humans to TZD treatment, we investigated whether TZDs have a differential efficiency in WAT of normal lean (OB/OB) versus pathological (ob/ob) mice. Treatment with rosiglitazone (RSG; 3 mg/kg/d) lowered plasma glucose, insulinemia, and, to a lesser extent, triglycerides in 10-week-old male ob/ob mice, but had no effect in OB/OB littermates (Supplemental Figure 1; supplemental material available online with this article; doi:10.1172/JCI38606DS1). This suggests that activation of PPARγ could induce distinct biological responses depending on the energetic status. To assess this at the molecular level, adipose tissue gene expression profiles were examined by oligonucleotide microarray analysis of visWAT mRNAs from OB/OB and ob/ob mice treated or not with RSG (Figure 1A). Although these tissues exhibited similar PPARγ protein expression levels (Figure 1B), RSG upregulated (>1.5-fold, $P < 0.05$) 32 genes in OB/OB visWAT, whereas 153 genes were upregulated in ob/ob visWAT, a substantial fraction of the latter being involved in metabolic control. Of these, only 4 genes were upregulated in both OB/OB and ob/ob visWAT, which suggests that PPARγ regulates distinct transcriptional networks in normal and pathological tissues. This was confirmed by a Gene Ontology functional classification. Importantly, upregulated genes in ob/ob visWAT included known direct target genes for PPARγ (e.g., *CIDEA*, *UCP1*, pyruvate carboxylase, and malic enzyme), which were not markedly upregulated in visWAT from OB/OB animals. We thus compared the ability of RSG to induce a subset of PPRE-driven adipocyte target genes in scWAT or visWAT from ob/ob mice and OB/OB littermates by real-time PCR. Whereas mRNA levels of the PPARγ target genes adiponectin (*Adpn*), glycerol kinase (*GyK*), *aP2*, *Glut4*, *Pparg*, and *PEPCK* were upregulated to a similar extent in scWAT from OB/OB and ob/ob mice, they exhibited a much stronger responsiveness to RSG in visWAT from ob/ob mice (Figure 1C), in line with the microarray data. These comparative results thus demonstrate that PPARγ target genes are more sensitive to agonist-mediated activation in obese than in lean visWAT. In sharp contrast, such an activity shift was not observed in scWAT.

RXRα protein steady-state levels are decreased in visWAT of obese, but not lean, humans and mice. PPARγ transcriptional activity depends on its association with a number of cofactors, including RXRs. We thus reasoned that the increased PPARγ transcriptional activity in obese visWAT might result from altered expression of a PPARγ cofactor. Preliminary characterization of the mRNA expression levels of several PPARγ primary cofactors did not reveal substantial differences between lean and obese visWAT, with the exception of *PGC1*, whose expression decreased by approximately 3-fold in obese visWAT (data not shown). We then monitored *Rxra*, *Rxrb*, and *Rxrg* mRNA levels by quantitative PCR (QPCR) in mouse scWAT and visWAT (Figure 2, A and B). *Rxr* mRNA levels were similar in WAT of OB/OB and ob/ob mice fed a regular diet (LFD) or high-fat diet (HFD). However, RXRα activity has previously been shown to be regulated by protein degradation in several cell types (31–35). We thus investigated whether RXRα polypeptide stability is affected in visWAT and scWAT of OB/OB and ob/ob mice. Immunohistochemical and Western blotting analyses revealed that RXRα was expressed in adipocytes and preadipocytes of both visWAT and scWAT from OB/OB mice (Figure 2C). We thus quantified the expression level of RXRα and RXRβ polypeptides, the highest expressed in OB/OB and ob/ob mouse visWAT and scWAT (Figure 2D). Western blot analysis of mouse WAT extracts for RXRα and RXRβ revealed that RXRα expression was strongly diminished in ob/ob visWAT, whereas RXRβ was expressed, although less abundantly so, at levels similar between OB/OB and ob/ob WAT (Figure 2, D–F). This altered expression was specific for visWAT; scWAT from OB/OB and ob/ob mice displayed similar RXRα and RXRβ levels. To rule out the possibility that RXRα downregulation is specific to the ob/ob genetic background, RXRα and RXRβ content was also quantified in WAT from mice fed either LFD or HFD. Interestingly, Rxrα, but not Rxrβ, protein levels were also specifically decreased in visWAT from HFD-fed mice (Figure 2, D–F). Similarly, we investigated whether RXR polypeptide stability is affected in human scWAT and visWAT biopsies from patients with different levels of obesity and diabetes (Figure 2, G and H). *RXRA*, *RXRB*, and *RXRG* mRNA levels did not differ between scWAT and visWAT biopsies from normal, obese, obese glucose intolerant, and obese diabetic individuals. Western blot analysis of WAT extracts revealed that RXRα, but not RXRβ, was much less abundant in visWAT from obese diabetic subjects than in visWAT from lean subjects (Figure 2, I–K). In contrast, *RXRA* and *RXRB* expression were not different in scWAT from lean and obese diabetic individuals (Figure 2, I–K).

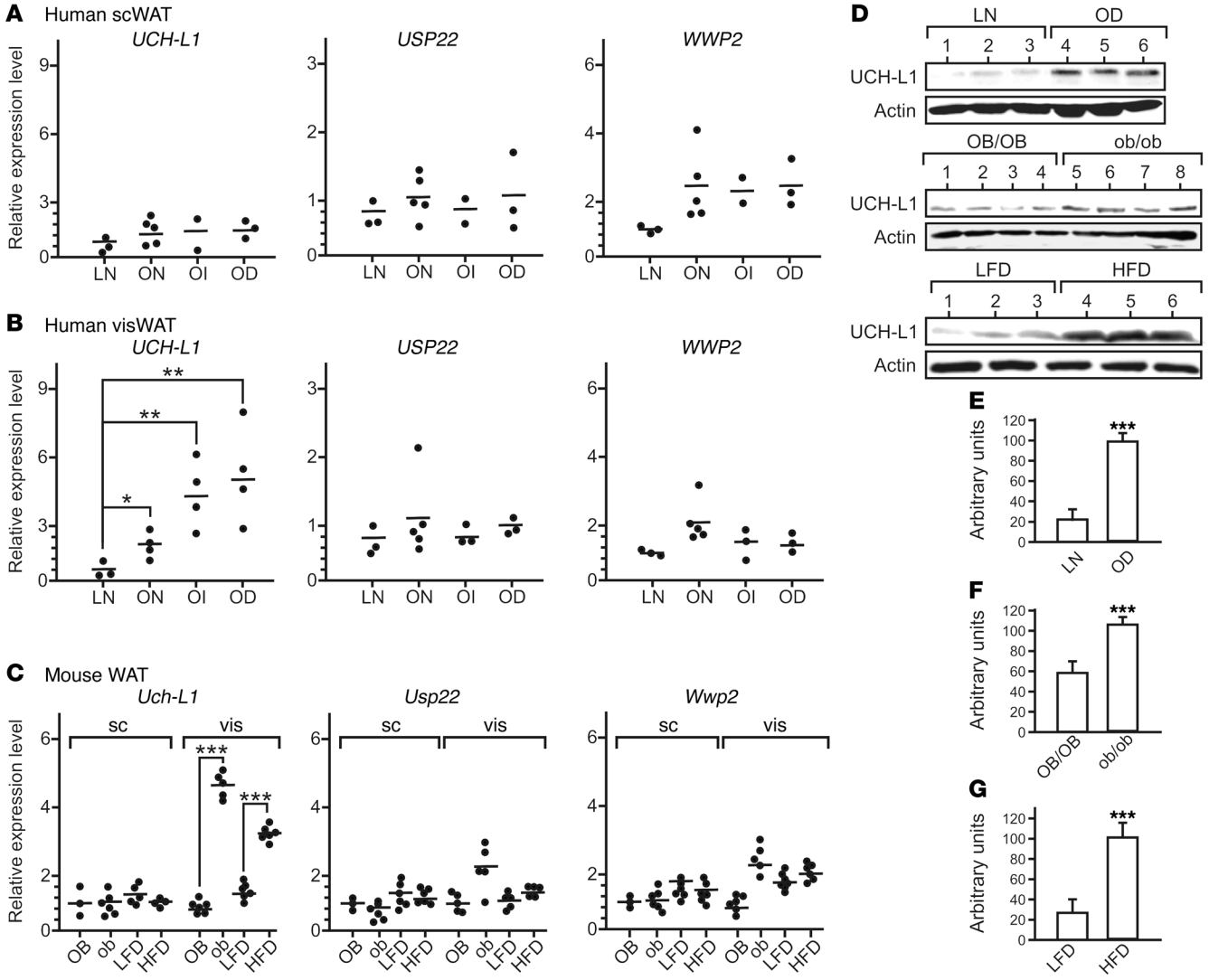

Figure 3

Expression of UCH-L1 is upregulated in visWAT from obese humans and mice. (**A**–**C**) Gene expression levels of *UCH-L1*, *USP22*, and *WWP2* were monitored by RT-QPCR using Taqman Assay on Demand sets of primers. Results are expressed relative to a control sample (LN for human WAT, OB/OB for mice) arbitrarily set to 1. (**D**) UCH-L1 protein expression in human and mouse WAT. Total protein extracts (50 g) were analyzed by Western blot and immunoprobed for UCH-L1. (**E**–**G**) Quantification of data in **D**. The intensity of each UCH-L1 band was normalized to actin. The first sample was arbitrarily set to 100%, and each sample was quantified relative to sample 1. Data represent mean SEM. $^{*}P < 0.05$, $^{**}P < 0.01$, $^{***}P < 0.005$.

Of note, PPARγ expression was comparable in all tissues (Figure 2, I and L). Collectively, these findings show that the RXRα protein is specifically degraded in visWAT from obese humans and mice.

Increased UCH-L1 expression in visWAT of obese humans and mice. Because *RXRA* mRNA levels were not altered, we postulated that the severe decrease in RXRα protein might stem from dysregulated expression of components of the UPS during metabolic disease progression. Therefore, UPS component expression was monitored in scWAT and visWAT from lean, obese, obese glucose intolerant, and obese diabetic individuals. Although the expression of components constituting the canonical 26S proteasome was not markedly altered in any of these WAT depots (data not shown), the expression of UCH-L1, an ubiquitin esterase/ligase enzyme, increased in visWAT, but not in scWAT, with progressing stages of the disease (Figure 3, A and B). In contrast, the expression of other UPS components, such as USP22 and WWP2 (known to regulate the stability of transcription factors such as NFκ-B or RNA polymerase 2), was not substantially modified. Because the dysregulated *UCH-L1* expression was depot specific in humans, we investigated whether a similar phenomenon occurs in mouse WAT tissues by comparing the expression of *Uch-L1*, *Usp22*, and *Wwp2* in WAT from OB/OB, ob/ob, LFD-fed, and HFD-fed mice (Figure 3C). Strikingly, a strong upregulation of *Uch-L1* mRNA was observed in visWAT tissues of ob/ob and HFD-fed mice, whereas *Usp22* and *Wwp2* exhibited less pronounced upregulation (5-fold versus 2.5-fold). In contrast, the expression of these genes was similar in scWAT of OB/OB, ob/ob, and HFD-fed mice. This upregulation was also observed at the

protein level (Figure 3D). These data demonstrate that *UCH-L1* is strongly and specifically upregulated in visWAT from metabolically challenged humans or mice.

RXRα polypeptide stability is altered by UCH-L1 upregulation and proteasomal degradation. The correlation between *UCH-L1* upregulation and the strongly reduced RXRα polypeptide steady-state levels in obesity led us to speculate that UCH-L1 could be critical in controlling RXRα stability. We therefore transfected 3T3-L1 preadipocytes with expression vectors coding for RXRα or RXRβ, with or without an expression vector coding for UCH-L1 (Figure 4A). Incubation of RXR-transfected cells with the proteasome inhibitor MG132 moderately increased the amount of RXRα, but did not influence RXRβ protein level. A combination of ammonium chloride and leupeptin (NH_4Cl/Leu), which inhibits the lysosomal degradation pathway, did not modify RXRα and RXRβ protein levels in RXR-transfected cells. Remarkably, UCH-L1 overexpression in RXR-transfected cells induced the breakdown of the RXRα polypeptide, whereas RXRβ stability was unaffected. UCH-L1–induced RXRα breakdown was prevented by MG132, but not by NH_4Cl/Leu, which indicates that UCH-L1 promotes RXRα breakdown through proteasomal degradation. RXR ubiquitinylation was then examined in 3T3-L1 preadipocytes transfected with expression vectors coding for RXR and HA-tagged ubiquitin. Immunoprecipitation of RXR followed by Western blot detection of HA-tagged ubiquitin (Figure 4B), or immunoprecipitation of HA-tagged proteins followed by Western blot detection of RXR (Supplemental Figure 2), showed that only RXRα was intensively conjugated to HA-ubiquitin and that UCH-L1 overexpression markedly increased ubiquitinylation of RXRα, but not RXRβ. Furthermore, an in vitro ubiquitinylation assay using purified RXRs as substrates showed that RXRα was ubiquitinated in an ATP-dependent manner (Figure 4C). Ubiquitin-conjugated RXRα was stabilized in the presence of ubiquitin aldehyde, a general inhibitor of ubiquitin hydrolases (36), or of MG132. In sharp contrast, RXRβ was not detectably conjugated to ubiquitin in similar conditions (Figure 4B and Supplemental Figure 2). Taken together, these data demonstrate that RXRβ is refractory to proteasome-mediated breakdown. Hypoxia is a feature of obese WAT (reviewed in ref. 37), characterized by induced gene expression and protein stabilization of hypoxia-inducible transcription factors (HIFs). Accordingly, *Hif1a* mRNA was upregulated in visWAT from ob/ob and HFD-fed mice (Figure 4D), whereas *Hif1b* and *Hif2b* expression was selectively increased in visWAT from HFD-fed mice. *Hif2a* expression was unaffected in both types of WAT. Because HIF1α upregulation in obese WAT correlated with increased *Uch-L1* expression (Figure 3C), and given the occurrence of several HIF-responsive elements in the promoter of the mouse and human *UCH-L1* genes, we tested whether cobalt chloride ($CoCl_2$), a hypoxia-mimicking compound, also upregulated UCH-L1 in differentiated 3T3-L1 adipocytes. $CoCl_2$ caused concomitant upregulation of *Hif1a* and *Uch-L1* mRNAs (Figure 4E) and dose-dependent degradation of the RXRα protein (Figure 4F). Furthermore, both MG132 and LDN-54777, a specific inhibitor of UCH-L1 (38), blocked the $CoCl_2$-induced RXRα degradation in a dose-dependent manner (Figure 4G). Pulse-chase labeling of 3T3-L1 adipocyte proteins showed that the decay of RXRα was linear, with a $t_{1/2}$ of about 8 hours (Figure 4H). $CoCl_2$ treatment decreased the $t_{1/2}$ of RXRα to 4 hours, whereas LDN-54777 clearly prevented the $CoCl_2$-induced RXRα breakdown ($t_{1/2}$, 7 hours). Taken together, these data argue for a role of UCH-L1 in the UPS-mediated RXRα degradation process, in which hypoxia might play a role.

The RXRα/RXRβ ratio determines PPARγ responsiveness to agonist in murine adipocytes. In light of the above results, we investigated whether an altered RXRα/RXRβ ratio might directly alter PPARγ responsiveness to agonist challenge in a cell-autonomous manner. Rxrα was strongly expressed in 3T3-L1 differentiated adipocytes, whereas Rxrβ and Rxrγ were expressed at much lower levels (Figure 5A). Pparγ, as well as Pparα, were also expressed in differentiated 3T3-L1 cells. RSG treatment readily activated *aP2*, *GyK*, and *Adpn* gene expression (Supplemental Figure 3). ChIP assays using anti-RXR or anti-PPAR antibodies (Figure 5B) failed to detect Rxrγ on the *aP2* and *Adpn* PPREs, in agreement with its low expression level, whereas comparable occupancy by both Rxrα and Rxrβ was detected on these promoters. Pparγ, but not Pparα, also bound to these promoters, and the density of Pparγ and RXRs on these promoters was similar in the absence and presence of RSG (Figure 5B). Identical results were obtained for the *GyK* promoter (data not shown). Thus, simultaneous expression of RXRα and RXRβ generates PPARγ-driven promoters on which both RXR isotypes can be loaded.

To further assess the role of the RXR isotype on *aP2*, *Adpn*, and *GyK* gene responsiveness to RSG, we generated Rxrα-depleted 3T3-L1 adipocytes by siRNA-mediated knockdown, which induced a specific *Rxra* mRNA decrease of 70% (Supplemental Figure 4). RXRα knockdown resulted in a more pronounced induction of the PPARγ target genes by RSG (*aP2*, 9.0- versus 3.6-fold; *Adpn*, 4.6- versus 2.6-fold; *GyK*, 6.3- versus 4.4-fold; Figure 5C). Conversely, 3T3-L1 CAR cells, which stably overexpress the adenovirus receptor (39), were differentiated into adipocytes and transduced at day 6 with adenoviral particles encoding GFP as a negative control, with Rxrα, or with Rxrβ, allowing for strong overexpression of each RXR isotype (Supplemental Figure 5). Interestingly, RSG treatment caused stronger induction of *aP2*, *Adpn*, *GyK*, and *Pparg* in RXRβ-overexpressing cells compared with GFP-expressing cells (Figure 5D). Inversely, forced expression of Rxrα attenuated the induction of Pparγ target genes by RSG (Figure 5D).

The RXRα/RXRβ ratio determines PPARγ responsiveness to agonist in different cellular backgrounds. We used QPCR analysis to investigate whether decreased Rxrα expression causes a derepression of PPARγ target genes in other cellular backgrounds that exhibit varying RXRα/RXRβ ratios (Figure 5E). 3T3-L1 preadipocytes displayed a *Rxra*/*Rxrb* mRNA ratio of 10:1, much like the HepG2 hepatocarcinoma and C2C12 myeloblastic cell lines (10:1 and 4:1, respectively). In contrast, the β-insulinoma cell line Min6 expressed comparable levels of *Rxra* and *Rxrb* mRNAs, at a 1:1 ratio. Assessment of the transcriptional activity of Pparγ in these different cell types using the J6 tk-Luc reporter gene showed that a much higher maximal transcriptional activity was reached in Min6 cells than in 3T3-L1, C2C12, and HepG2 cells in response to RSG (Figure 5F). Overexpressing Rxrα in Min6 cells significantly blunted the response to RSG, whereas overexpression of Rxrβ potentiated this response (Figure 5G). A similar pattern was obtained in COS cells and on another PPRE-driven reporter gene, ApoA2 tk-Luc, which demonstrates that the RXRα-repressive function was dependent neither on the cell type nor on the response element (Figure 5H). We then used a system in which the P box, located in the DNA-binding domain (DBD) of either Rxrα or Rxrβ, was mutated to confer a high affinity for a glucocorticoid-responsive element (GRE) half site. The RXR binding polarity can thus be imposed when using a chimeric direct repeat 1 response element PPRE in which the GRE half site is located in either 3′ or 5′. This system was only functional when RXR was

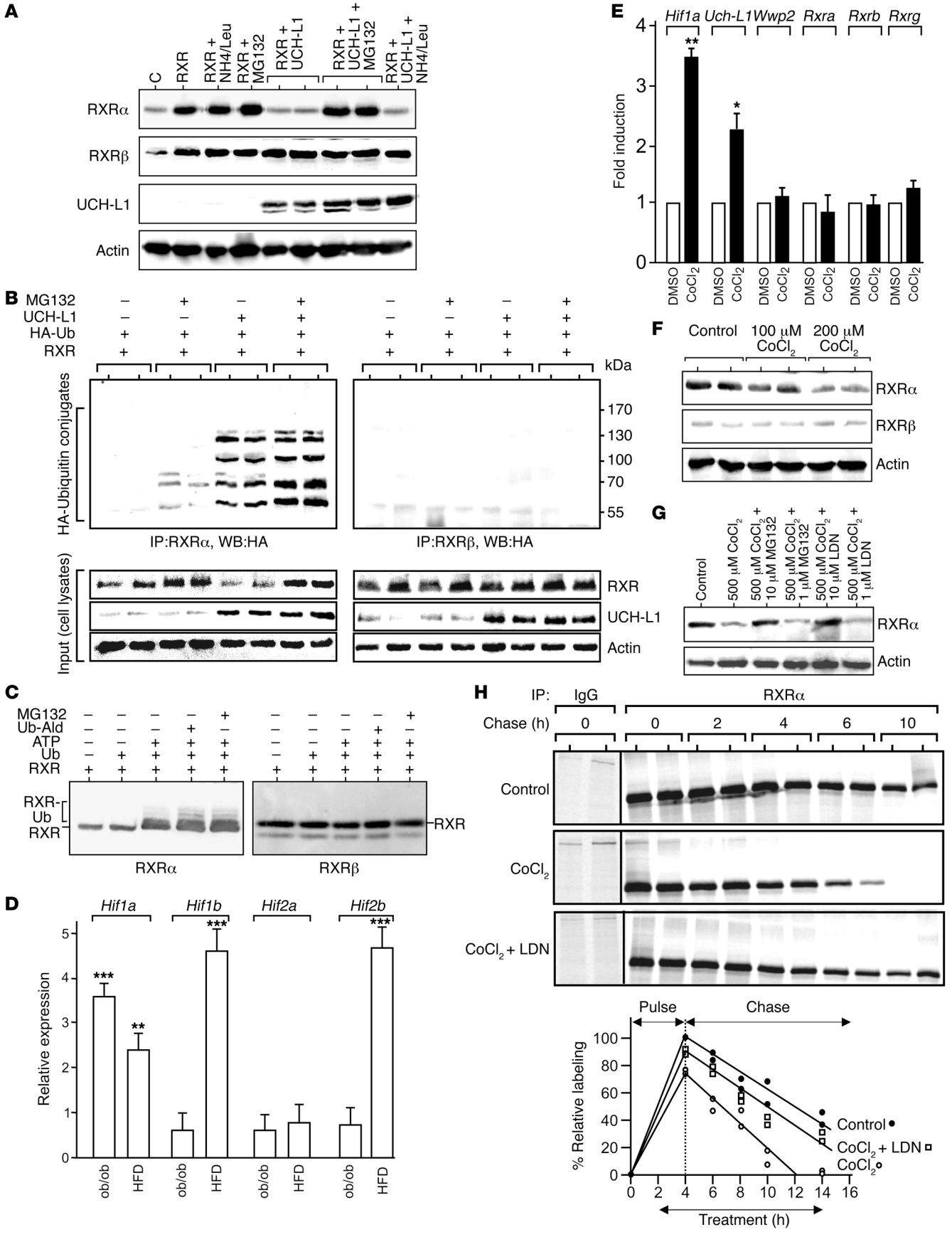
A
C
RXR
RXR + NH4/Leu
RXR + MG132
RXR + UCH-L1
RXR + UCH-L1 + MG132
RXR + UCH-L1 + NH4/Leu
RXRα
RXRβ
UCH-L1
Actin
B
MG132
UCH-L1
HA-Ub
RXR
kDa
HA-Ubiquitin conjugates
170
130
100
70
55
IP:RXRα, WB:HA
IP:RXRβ, WB:HA
Input (cell lysates)
RXR
UCH-L1
Actin
C
MG132
Ub-Ald
ATP
Ub
RXR
RXR-Ub
RXR
RXRα
RXRβ
D
Hif1a
Hif1b
Hif2a
Hif2b
Relative expression
ob/ob
HFD
E
Hif1a
Uch-L1
Wwp2
Rxra
Rxrb
Rxrg
Fold induction
DMSO
CoCl2
F
Control
100 μM CoCl2
200 μM CoCl2
RXRα
RXRβ
Actin
G
Control
500 μM CoCl2
500 μM CoCl2 + 10 μM MG132
500 μM CoCl2 + 1 μM MG132
500 μM CoCl2 + 10 μM LDN
500 μM CoCl2 + 1 μM LDN
RXRα
Actin
H
IP:
IgG
RXRα
Chase (h)
0
2
4
6
10
Control
CoCl2
CoCl2 + LDN
Pulse
Chase
% Relative labeling
Control
CoCl2 + LDN
CoCl2
Treatment (h)

Figure 4
RXRα is selectively degraded through the ubiquitin proteasome system. (**A**) 3T3-L1 preadipocytes were transfected with expression vectors coding for UCH-L1, RXRα, or RXRβ, then treated with 10 μM MG132 or 10 μM NH_4Cl/Leu overnight. Whole cell extracts were prepared 48 hours after transfection and analyzed by Western blot. C, control. (**B**) In vivo ubiquitin conjugation of RXRα or RXRβ in 3T3-L1 preadipocytes. Cells were transfected as above with an additional expression vector coding for HA-tagged ubiquitin (Ub) and treated as in **A**. Whole cell extracts were submitted to immunoprecipitation with an anti-RXR antibody followed by Western blot analysis of HA-conjugated proteins. (**C**) In vitro ubiquitinylation of RXRα and RXRβ. Purified recombinant RXRα or RXRβ (50 ng) was incubated for 4 hours with ubiquitin (100 μg/ml), ATP (0.5 mM), ubiquitin aldehyde (Ub-Ald; 20 μg/ml), or MG132 (10 μM) and analyzed by Western blotting. (**D**) HIF transcription factor mRNA levels in mouse visWAT. *Hif1a*, *Hif1b*, *Hif2a*, and *Hif2b* mRNAs were quantified by RT-QPCR. Expression levels are shown relative to control OB/OB or LFD WAT as appropriate, arbitrarily set to 1. (**E**) Gene expression levels in 3T3-L1 adipocytes upon $CoCl_2$ treatment for 4 hours. (**F**) RXR protein levels in 3T3-L1 adipocytes upon $CoCl_2$ treatment for 16 hours. (**G**) Proteasome and UCH-L1 inhibition protected Rxrα from CoCl2-induced degradation. 3T3-L1 adipocytes were treated for 16 hours as indicated, and whole cell extracts were analyzed by Western blotting. (**H**) Pulse-chase labeling of Rxrα in 3T3-L1 adipocytes. Adipocytes were treated as described in Methods. Labeled *Rxra* was immunoprecipitated and quantified by autoradiography.

bound on the 3′ half site of the chimeric PPRE (ref. 40 and Figure 5I). In this configuration, Pparγ was more sensitive to a moderate 30-nM concentration of RSG when Rxrβ was expressed (Figure 5I).

Taken together, these data indicate that (a) PPARγ can bind as a dimer with RXRα or RXRβ to PPRE-driven promoters in adipocytes; (b) this interaction is not ligand sensitive; and (c) decreased RXRα expression correlates in vitro and in vivo to an increased responsiveness to RSG. RXRα thus acts as a repressor of PPARγ responsiveness to agonist challenge in murine adipocytes.

Corepressors interact with PPARγ in vitro and in intact cells. Collectively, these results show that PPARγ-RXRα heterodimers display lower sensitivity to agonist challenge than do PPARγ-RXRβ dimers. To test whether this might be the result of increased interaction with corepressors, the influence of the RXR isotype on the binding of PPARγ to SMRT or NCoR was further characterized. A yeast 2-hybrid assay was first performed to assess the interaction of PPARγ fused to the Gal4 DBD, with the NR interaction domain (NRID) of either SMRT (aa 2,061–2,472) or NCoR (aa 1,906–2,313) fused to the NF-κB activation domain. SMRT interacted more efficiently with the PPARγ LBD than did NCoR, whereas interaction of the PPARγ LBD with the coactivator Med1 (also known as TRAP220 or DRIP205) was negligible (Figure 6A). A similar 2-hybrid assay in mammalian HeLa cells using the PPARγ LBD fused to the Gal4 DBD and NRIDs fused to the VP16 activation domain (VP16-AD) revealed a similar pattern of interaction (Figure 6B), demonstrating that the preferential interaction of SMRT with PPARγ is an intrinsic property not affected by the cellular background. SMRT was therefore selected as the representative corepressor in further experiments.

A glutathione S-transferase–pulldown (GST-pulldown) assay was then carried out to assess the interaction between full-length PPARγ and SMRT. Using an immobilized GST-SMRT fusion protein and radiolabeled PPARγ, we detected a strong interaction between the proteins in this system (Figure 6C). RSG (Figure 6C) and 2 other PPARγ agonists, pioglitazone and troglitazone (Supplemental Figure 6A), were unable to promote significant release of SMRT from monomeric PPARγ. In similar conditions, RSG promoted the recruitment of Med1, GRIP1 (also known as TIF-2), and PGC-1α to the PPARγ LBD (Supplemental Figure 6B), showing that the PPARγ LBD undergoes appropriate structural transitions. Thus, the PPARγ-SMRT interaction was not sensitive to PPARγ agonist binding in this setting. To assess whether a stable interaction with SMRT also occurred on PPARγ target gene promoters, ChIP assays were performed in 3T3-L1 adipocytes. 3T3-L1 cells express several coactivators, as well as NCoR and SMRT, whose mRNA expression levels did not vary significantly during the differentiation process (Supplemental Figure 7). In differentiated, unstimulated 3T3-L1 adipocytes, SMRT was clearly detected on each promoter, whereas NCoR displayed barely detectable binding (Figure 6D). Upon RSG treatment, SMRT was partially dismissed from both promoters, which indicates that, in the context of an endogenous functional promoter, agonist-activated PPARγ is able to at least partially release SMRT. To confirm these findings, we monitored the association of 2 SMRT-associated proteins, HDAC3 and SIRT1. Similar to SMRT, both HDAC3 and SIRT1 were partially dismissed from the *aP2* and *Adpn* promoters (Figure 6E). Thus a partial, agonist-induced dismissal of corepressor complex correlated with mixed RXRα/RXRβ occupancy at PPARγ-regulated target genes (Figure 5B).

RXR isotype affects SMRT interaction with the PPARγ-RXR heterodimer. We hypothesized that the observed increase in PPARγ-RXRβ responsiveness to agonist could result from a specific feature of the RXRα-SMRT interaction. This hypothesis was tested using a 2-hybrid assay in NIH-3T3 cells, which expresses neither PPARγ nor C/EBPα, but can be fully differentiated into adipocytes upon ectopic expression of these 2 transcription factors (ref. 41 and Figure 7A). A Gal4-SMRT NRID fusion protein was overexpressed together with a PPARγ LBD–VP16-AD fusion protein in the presence or absence of RXRα or RXRβ. The transcriptional activity of the system was monitored with a UAS tk-Luc reporter gene, whose activity was predicted to decline upon dissociation of the PPARγ-VP16 protein. As a control experiment, we expressed a human RAR-VP16 (hRAR-VP16) fusion protein together with the Gal4-SMRT NRID. This system displayed clear agonist-dependent decreased transcriptional activity (*all trans* retinoic acid; atRA), reflecting the dissociation of the hRAR-VP16 fusion protein from the Gal4-SMRT bait upon agonist binding (Figure 7A). In similar conditions, the PPARγ-VP16–Gal4-SMRT interaction was not sensitive to increasing concentrations of RSG. Concomitant overexpression of RXRα, RXRβ, or RXRγ increased the basal level of interaction of PPARγ with SMRT. However, RSG decreased system activity only in the presence of RXRβ, which indicates decreased SMRT association with the PPARγ-RXRβ heterodimer. Taken together, these data suggest that the PPARγ-SMRT interaction is disrupted by RSG only when RXRβ is integrated in the ternary SMRT-PPARγ-RXR complex.

RXR isotype affects SMRT-mediated repression of PPARγ. We concluded from ChIP and 2-hybrid data that the PPARγ-RXRα interaction with SMRT was ligand insensitive. To further validate this hypothesis in the context of a DNA-bound PPARγ-RXR heterodimer, we used a modified 2-hybrid assay in NIH 3T3 cells. The J6 tk-Luc reporter gene was cotransfected with PPARγ and RXR expression vectors, together with an expression plasmid coding either for VP16-AD as a control or for a SMRT–VP16-AD fusion protein (Figure 7B). Preliminary experiments showed that detected responses necessitated a PPRE sequence (data not shown). We first used the RARα-RXRα heterodimer as a control system. The basal activity of this dimer strongly increased in the presence of VP16-SMRT, indicative of a

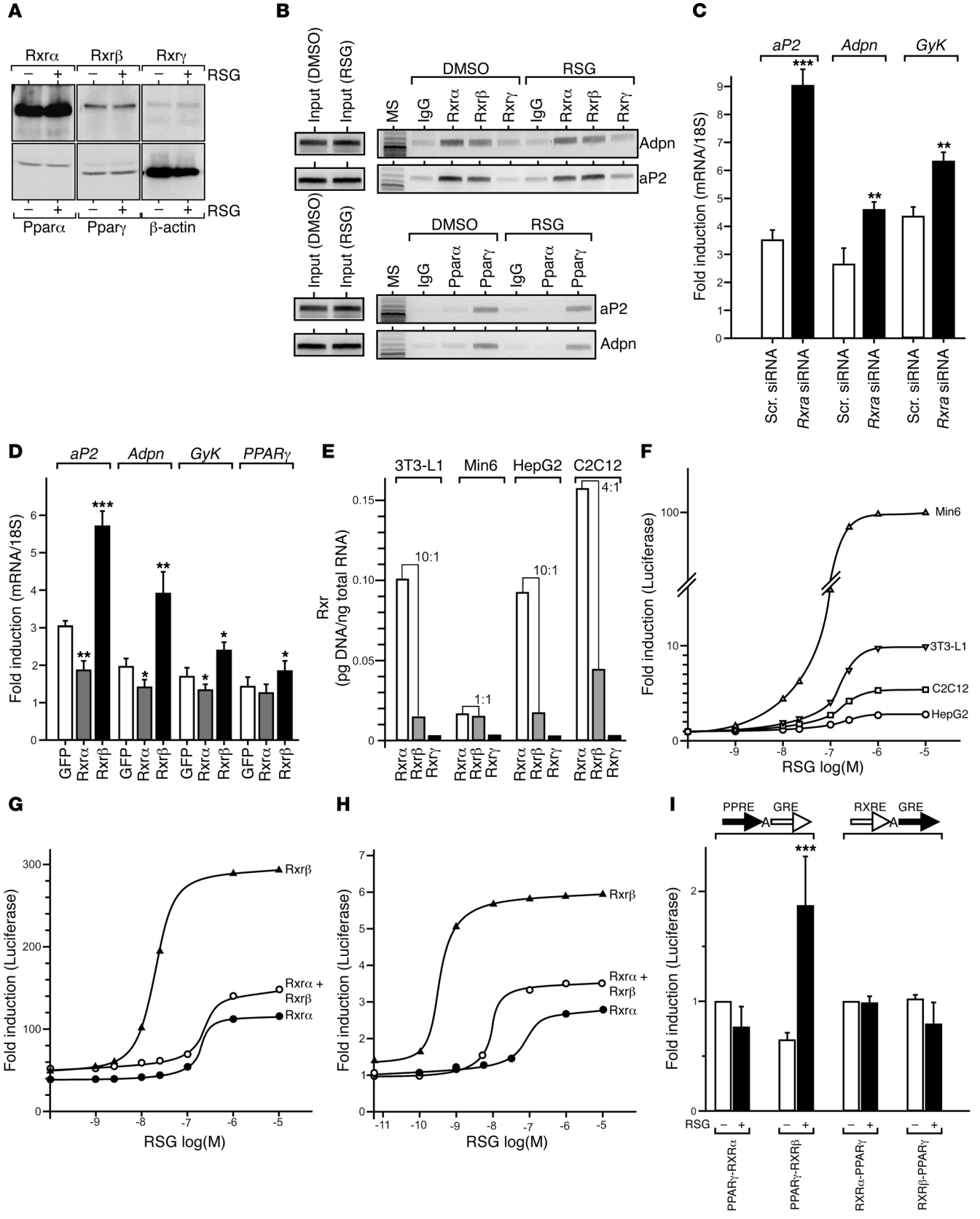
A
Rxrα
Rxrβ
Rxrγ
RSG
Pparα
Pparγ
β-actin
B
Input (DMSO)
Input (RSG)
DMSO
RSG
MS
IgG
Adpn
aP2
C
aP2
Adpn
GyK
Fold induction (mRNA/18S)
Scr. siRNA
Rxra siRNA
D
PPARγ
GFP
E
3T3-L1
Min6
HepG2
C2C12
Rxr
(pg DNA/ng total RNA)
10:1
1:1
4:1
F
Fold induction (Luciferase)
RSG log(M)
G
H
I
PPRE
GRE
RXRE
PPARγ-RXRα
PPARγ-RXRβ
RXRα-PPARγ
RXRβ-PPARγ

Figure 5
RXRα exerts a repressive effect on PPARγ-mediated transcription. (**A**) RXR and PPAR isotype expression in differentiated 3T3-L1 adipocytes. Whole cell extracts (50 g) from control or RSG-treated (2 hours) cells were analyzed by Western blotting. (**B**) Promoter occupancy by RXR and PPAR isotypes. Differentiated 3T3-L1 cells were treated as in **A**. RXR and PPAR association to the *aP2* and *Adpn* PPREs was detected by ChIP assay. (**C**) Rxrα knockdown enhanced Pparγ responsiveness to RSG in 3T3-L1 adipocytes. 3T3-L1 adipocytes were transfected with control, scrambled, or anti-*Rxra* siRNAs and treated with 1 μM RSG 24 hours later. mRNAs were assayed by QPCR for *aP2*, *Adpn*, and *GyK* transcripts. Results are expressed relative to untreated cells. Data represent mean ± SEM ($n = 3$). $^{**}P < 0.01$, $^{***}P < 0.005$. (**D**) Overexpression of RXRα blunted induction of PPARγ target genes in 3T3-L1 CAR adipocytes. 3T3-L1 CAR cells were differentiated and transduced at day 5 with adenovirus encoding GFP, Rxrα, or Rxrβ. mRNA quantification at day 7 was as in **C**. Data represent mean ± SEM ($n = 3$). $^{**}P < 0.01$, $^{***}P < 0.005$. (**E**) Expression levels of RXR isotypes in Min6, 3T3-L1, HepG2, and C2C12 cells. Total RNA from each cell type was analyzed by QPCR for their absolute content in RXR mRNAs. (**F**) Min6, undifferentiated 3T3-L1, C2C12, and HepG2 cells were transfected with the PPRE-driven J6 tk-Luc reporter gene and stimulated with increasing concentrations of RSG. Luciferase activities are expressed relative to basal expression of the unstimulated reporter system (DMSO), arbitrarily set to 1. (**G**) Rxrα overexpression blunted Pparγ responsiveness to RSG in Min6 cells. Min6 cells were transfected with the J6 tk-Luc reporter gene and with 30 ng of either RXRα or RXRβ expression vector or 15 ng of each. Luciferase activities were assayed and graphed as in **F**. (**H**) Rxrα overexpression blunted Pparγ responsiveness to RSG in COS cells. Experimental conditions were as in **F**. (**I**) RXRβ confers RSG responsiveness to a positionally restricted PPARγ-RXR heterodimer. PPARγ and mutated RXRα or RXRβ (both binding to a glucocorticoid response element half site; ref. 61) were overexpressed in HeLa cells, and the transcriptional activity of the heterodimer was monitored using a reporter gene driven by a composite GRE-PPRE or PPRE-GRE tk-Luc reporter gene. Results are expressed as in **F**. Data represent mean ± SEM ($n = 3$). $^{***}P < 0.005$.

hRARα-RXRα–SMRT interaction. A saturating concentration of atRA (1 μM) yielded luciferase activity similar to that observed in control conditions, showing that SMRT was fully dissociated from the RXR-RAR complex upon agonist binding (Figure 7B). When transposed to the PPARγ-RXRα system, VP16-SMRT expression also strongly increased the basal activity of the reporter gene (5-fold induction) compared with VP16-AD alone. However, in contrast to the RXRα-RARα dimer, higher transcriptional activity of the PPARγ-RXRα dimer compared with control conditions was maintained even at a saturating RSG concentration. This additive induction was a result of the cumulative effect of the AF2- and VP16-mediated transcriptional activation domains, strongly suggesting that agonist treatment does not induce the dismissal of VP16-SMRT from the PPARγ-RXRα heterodimer. RXRγ exhibited behavior similar to that of RXRα (Figure 7C). In sharp contrast, RXRβ overexpression generated a system in which saturating RSG concentrations prevented SMRT-VP16 from further activating the reporter gene activity, showing that the liganded PPARγ-RXRβ dimer cannot bind the SMRT moiety. We conclude from the above data that only the PPARγ-RXRβ dimer fully releases SMRT upon agonist binding.

Discussion

The transcriptional control of programs regulating metabolic homeostasis can be substantially altered by manipulating the activity of transcription factors belonging to the NR superfamily. Among the NRs, PPARγ plays an important role as a central regulator of lipid and glucose metabolism and is important for maintaining whole-body insulin sensitivity (42). However, how its function may be modulated upon disease progression is unknown. Our results provide what we believe to be a novel paradigm on how a transcriptional regulator may adjust its transcriptional activity in the face of metabolic challenges.

The inverse correlation in visWAT from obese mice and humans between *UCH-L1* expression and RXRα polypeptide stability highlights a regulatory mechanism of the PPARγ signaling pathway. UCH-L1 exhibits ubiquitin C-terminal hydrolase activity, which, by maintaining a sufficient pool of cellular ubiquitin, sustains protein degradation. Additional roles, such as ubiquitin ligation and stabilization of monoubiquitin, have previously been described for UCH-L1 (reviewed in ref. 43). UCH-L1 substrates are unknown, but its involvement in regulating NF-κB activity in vascular cells (44) and its varied gene expression in rat pancreatic islets exposed to high glucose concentrations (45) hint at a role in metabolic control. Although we found increased UCH-L1 expression at various stages of disease progression in humans, the mechanism leading hereto is unknown. Hypoxia, which affects obese WAT (37), may be a possible link between pathological states and increased *UCH-L1* expression. In addition, hypoxia has been reported to promote RXRα breakdown in cardiac myocytes (46). In ob/ob and HFD visWAT, we observed increased expression of *Hif1a*, and the UCH-L1 promoter contains several HIF-responsive elements. In agreement with these observations, $CoCl_2$, an agent mimicking partially hypoxia through HIF1α induction and stabilization, was found to increase UCH-L1 expression in 3T3-L1 adipocytes and to promote RXRα protein breakdown in a UCH-L1–dependent manner. RXRα is a known target of the UPS in several cell types (31–35), and our present data showed that RXRα was a substrate for in vitro ubiquitin conjugation, whereas RXRβ was unable to undergo this posttranslational modification. However, recombinant UCH-L1 neither modified the ubiquitin conjugation rate in the acellular system nor engaged direct protein-protein interaction with RXRα in vitro, as assayed by GST-pulldown assays (data not shown), which suggests that this enzyme promotes RXRα breakdown in an indirect manner. Combined with the fact that visWAT from ob/ob mice is more sensitive to TZD treatment than is visWAT from OB/OB mice, our data raised the possibility that an UCH-L1–dependent RXR expression isotype switch could control PPARγ transcriptional activity.

As with all other ligand-regulated NRs, PPARγ exerts its transcriptional activity through the recruitment of coactivators, and PPARγ has been documented to bind in vitro to a variety of primary coactivators. PPARγ transcriptional activity is also modulated by corepressor recruitment, and we showed here that PPARγ-containing heterodimers preferentially recruited SMRT over NCoR. Such a preference has been reported by some in a variety of cell-free and cellular systems (25, 40, 47, 48), but not confirmed by others (26, 49). Although RNA interference studies showed that SMRT repressed PPARγ transcriptional activity (data not shown), we found that the physical interaction of PPARγ with SMRT was not affected by agonist binding. Thus, assays involving solely PPARγ lack a critical component required for the ligand-regulated association of SMRT to PPARγ, in line with a previous report (50). As an obligate heterodimerization partner conferring specific DNA binding activity to PPARγ, RXR is a major regulator of PPARγ activity. Mammalian 2-hybrid assays established that RXR association to PPARγ allowed for a reversible association of SMRT to the PPARγ-RXR heterodimer

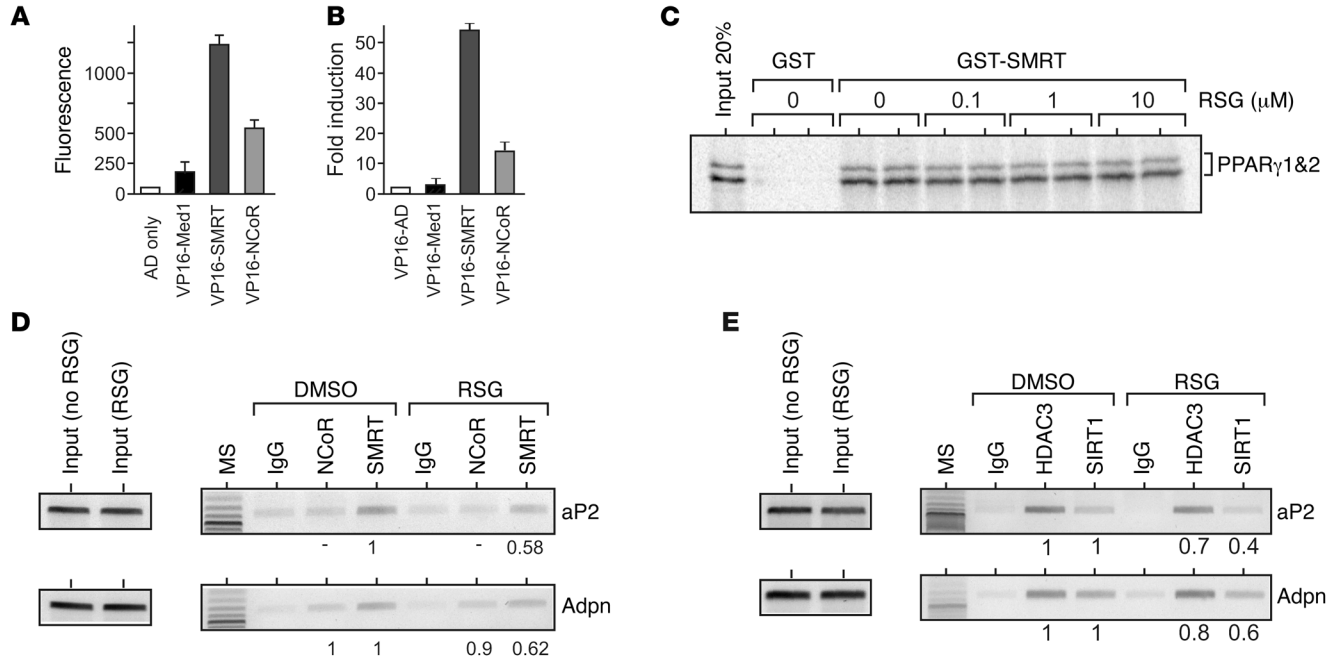

Figure 6

Ligand-dependent dismissal of SMRT from PPARγ depends on its association with RXR isotypes. (**A**) Cofactor interaction in yeast. Vectors encoding for the VP16-AD alone (AD only), or in frame with the NRID of Med1 (VP16-Med1), SMRT (VP16-SMRT), or NCoR (VP16-NCoR), were coexpressed with the PPARγ LBD fused to the Gal4 DBD. Fluorescence is expressed as arbitrary units. (**B**) Cofactor interaction in mammalian cells. An experimental strategy similar to that described in **A** was used to monitor Med1, SMRT, or NCoR interaction with the PPARγ LBD in HeLa cells. The basal level observed in the presence of VP16-AD and Gal4-PPARγ LBD was arbitrarily set to 1. (**C**) SMRT interaction with PPARγ LBD in a cell-free system. A GST-SMRT fusion protein was incubated with radiolabeled PPAR1 and PPAR2, with increasing concentrations of RSG. GST-SMRT–PPARγ complexes were resolved by SDS-PAGE and autoradiographed. (**D**) Corepressor interaction with aP2 or Adpn promoters in adipocytes. ChIP assays were carried out in differentiated 3T3-L1 cells to detect SMRT or NCoR loading to the aP2 or Adpn promoters. All experiments were carried out at least 3 times. (**E**) Promoter occupancy by deacetylases. ChIP assays were carried out as in **D** to detect either SIRT1 or HDAC3 binding to the aP2 or Adpn PPREs. Numbers below blots indicate level of binding relative to DMSO control, arbitrarily set to 1.

in an isotype-dependent manner. Only RXRβ generated a complex able to dismiss SMRT in an agonist-dependent manner, providing a molecular basis for the higher inducibility of PPARγ in RXRβ-enriched cellular backgrounds. This was also true in a mouse adipocyte background, in which RXRα and RXRβ normally associate to the PPRE of PPARγ target genes. The interaction of PPARγ, as well as that of RXRs, with the PPRE of the endogenous *aP2*, *Adpn*, and *GyK* gene promoters was constitutive and ligand insensitive in differentiated 3T3-L1 adipocytes, in agreement with previous data (26). The mixed composition of PPRE-bound heterodimers, in light of our interaction data, led us to predict that SMRT would be only partially released upon agonist challenge. This was indeed the case, confirmed by the partial release of SMRT-interacting proteins HDAC3 and Sirt1. In agreement with the repressive role of RXRα, siRNA-mediated decrease of RXRα expression led to a higher sensitivity to RSG; conversely, its overexpression in 3T3-L1 adipocytes and other cellular backgrounds invariably blunted responsiveness to RSG. A differential affinity of NRs for distinct corepressors has only been documented for NRs expressed as monomers. For example, restricted SMRT recruitment has been observed for the atRA receptors RARα, RARβ, and RARγ (51, 52), and differences are due to the poorly conserved C-terminal F domain (53). However, since neither RXRs nor PPARγ have an F domain, other structural determinants must regulate the differential affinity of RXRα- versus RXRβ-containing heterodimers for SMRT and are yet to be identified.

It has been postulated that the tissue-specific recruitment of nuclear coactivators by specific agonists influences PPARγ transcriptional activity, a mechanism by which side effects triggered in TZD target tissues, such as kidney, bone, or even adipose tissues, could be circumvented (e.g., refs. 54–56). Our data suggest that PPARγ operates differently in normal and pathological tissues as a result of heterodimerization with distinct RXR isotypes. Whether this phenomenon also impinges on the ability of PPARγ to recruit a specific subset of coactivators is unknown, but nevertheless underlines the need for a careful selection of screening procedures aimed at identifying novel PPARγ synthetic ligands. It also leaves open the possibility to design ligands favoring — or not — heterodimerization with RXRα, thereby predictably moderating the transcriptional response to synthetic PPARγ ligands. The need for moderated PPARγ activation has already been underlined by (a) the protective effect of the transcriptionally altered Pro12Ala PPARγ mutant against the development of insulin resistance and T2DM; (b) the improved insulin sensitivity of heterozygous PPARγ mice fed a HFD; and (c) the beneficial effects on obesity and insulin resistance upon treatment with PPARγ antagonists (57).

In summary, our studies elucidated an unexpected mechanism by which the UPS regulates PPARγ transcriptional activity in pathological states through selective degradation of RXRα. Modifying PPARγ transcriptional activity in the face of metabolic challenges may be a mechanism by which cells adapt to novel conditions through tran-

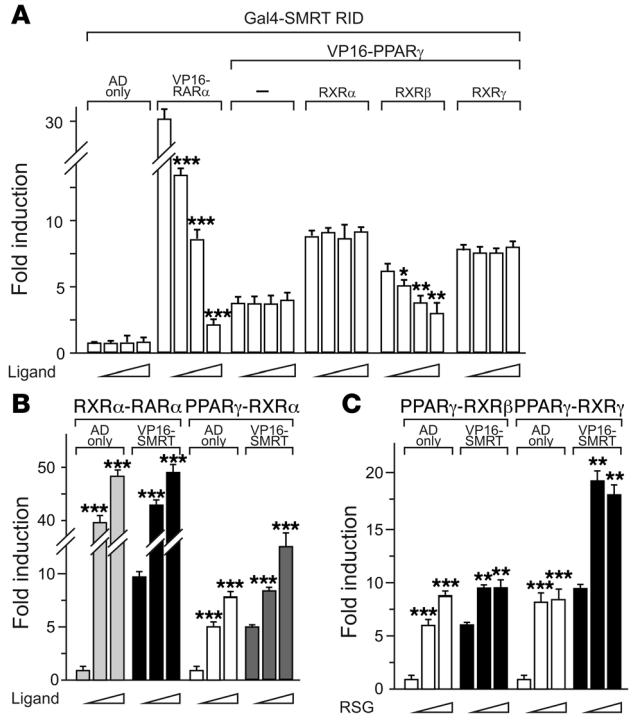

Figure 7
RXRα overexpression confers ligand sensitivity to the SMRT-PPARγ interaction. (**A**) NIH 3T3 fibroblasts were transfected with expression vectors coding for the fusion protein Gal4-SMRT NRID, the full-length PPARγ fused to the VP16-AD (VP16-PPARγ), and each RXR isotype. The full-length RARα fused to VP16-AD (VP16-RARα) was used as a positive control. The basal level observed in the presence of the VP16-AD and Gal4-SMRT NRID was arbitrarily set to 1. The reporter gene was a pGL3-based vector containing 6 repeats of the UAS yeast sequence. (**B**) Interaction of SMRT with the PPRE-bound PPARγ-RXRα heterodimer. NIH 3T3 cells were transfected with the expression vectors and reporter gene as in **A**, together with an expression vector coding for the VP16-AD or the VP16-AD fused to the SMRT NRID (VP16-SMRT). At 24 hours after transfection, increasing concentrations of RSG (0, 1, or 5 μM) were added for 16 hours, and luciferase activities were assayed and quantified as in **A**. The RXRα-RARα heterodimer was used as a positive control in response to 0.5 or 1 μM atRA. (**C**) Interaction of SMRT with the PPRE-bound PPARγ-RXRβ or the PPARγ-RXRγ heterodimer. Transient transfection experiments were carried out as described as in **B** using either a RXRβ or a RXRγ expression vector. Data represent mean ± SEM. $n = 3$. $^*P < 0.05$, $^{**}P < 0.01$, $^{***}P < 0.005$.

scriptional reprogramming. Whether RXRα- and RXRβ-containing heterodimers control an overlapping or a specific transcriptional program is under investigation. A better understanding of the as-yet putative specific roles of RXR isotypes and of their regulation in pathological conditions may help define new therapeutical strategies to treat T2DM and associated comorbidities.

Methods

Chemicals. Isobutylmethylxanthine (IBMX), insulin, dexamethasone, and atRA were obtained from Sigma-Aldrich. LDN-57444 was purchased from Calbiochem. RSG was synthesized at the chemical facilities at Institut de Recherches Servier.

Plasmids. pSG5-hRAR, pSG5-hRXR, pSG5-hRXR, pSG5-hRXR, pSG5-hPPARγ (DR5)3-tk Luc, VP16-hRAR (PPRE)6-tk Luc, and Gal4-tk Luc were described elsewhere (58–61). VP16-PPARγ was provided by B.M. Forman (City of Hope National Medical Center, Duarte, California, USA; ref. 62). Gal4-hSMRT$_{2117–2357}$ and VP16-hSMRT$_{2117–2357}$ were gifts from A.N. Hollenberg (Beth Israel Deaconess Medical Center, Boston, Massachusetts, USA; ref. 25). pCMX-VP16-NCoR$_{1585–2453}$ was provided by R. Renkawitz and M. Schulz (Institute for Genetics, Giessen, Germany; ref. 63). The pCMV-based human UCH-L1, USP22, and WWP2 expression vectors were purchased from OriGene.

Cell culture and transfection. NIH 3T3 cells were grown in DMEM (Glutamax-1, high glucose; Invitrogen) supplemented with 10% FCS (BioWhittaker) and 100 U/ml penicillin and 100 μg/ml streptomycin (Invitrogen). Transient transfection experiments were performed using Lipofectamine 2000 (Invitrogen). Luciferase assays were performed with the dual luciferase assay system (Promega) according to the manufacturer's guidelines.

Adipocyte differentiation was induced as follows: 3T3-L1 preadipocytes were cultured in DMEM supplemented with 10% FCS until they reached confluence. The medium was then changed, and cells were allowed to grow for 2 additional days. Adipocyte differentiation was then induced by replacing the culture medium by DMEM supplemented with 10% FCS, 0.5 mM IBMX, 1 μM dexamethasone, and 10 μg/ml insulin. 2 days later, the medium was replaced with DMEM supplemented with 10% FCS and 10 μg/ml insulin for 2 additional days. Cells were then refed at 48-hour intervals with DMEM supplemented with 10% FCS only.

Pulse-chase labeling and immunoprecipitation. Differentiated 3T3-L1 cells were starved in methionine/cysteine-free DMEM supplemented with glutamine and 10% dialyzed FCS for 4 hours. [^{35}S] methionine and cysteine (250Ci, EasyTag EXPRESS^{35}S Protein Labeling Mix; Perkin-Elmer) was added to the culture medium for 4 hours. At 2 hours prior to the end of the pulse, 500 μM $CoCl_2$ and/or 10 μM LDN-57444 was added to the medium. Radioactive media was removed and substituted for regular medium supplemented with 2 mM cysteine and methionine, $CoCl_2$, and/or LDN-57444. At the indicated times, approximately 10^7 cells were collected in ice-cold 1× PBS, centrifuged, and lysed into 500 μL RIPA buffer (50 mM Tris-HCl, pH 7.4; 150 mM NaCl; 1% NP-40; 0.5% deoxycholate; 0.1% SDS; 10 μg/ml leupeptin; 10 μg/ml pepstatin; 5 μg/ml aprotinin; 5 mM DTT; 5 mM PMSF; and 1 mM benzamidine). The homogenate was spun down, and the supernatant was precleared with a protein A/protein G sepharose mix. The supernatant was incubated overnight at 4°C with 5 μg anti-RXRα antibody (ΔN-197, sc-774; Santa Cruz Biotechnology Inc.). Complexes were precipitated with a protein A/protein G mix, washed, and analyzed by 8% SDS-PAGE.

In vitro ubiquitin conjugation. In vitro ubiquitinylation assays were carried out using a S100 HeLa cell extract and reagents according to the manufacturer's instructions (Enzo Life Sciences).

In vivo ubiquitin conjugation. 3T3-L1 preadipocytes were transfected with expression vectors encoding HA-tagged ubiquitin (MT123-Ub HA; refs. 64, 65), RXRα, or RXRβ. At 24 hours after transfection, whole cell extracts were prepared in RIPA buffer supplemented with 10 μM MG132, and HA-tagged proteins were immunoprecipitated using an anti-HA tag antibody (ab9110; Abcam) or anti-RXR antibodies (see below). Ubiquitinylated RXR was detected by Western blotting using either anti-RXR or anti-HA tag antibodies as indicated in the figure legends.

Immunofluorescence and Western blot. The anti-RXRα antibody used in immunochemistry experiments was from Perseus (PP-K8508-00). WAT was embedded in paraffin and sectioned (7 μm). Sections were deparaffinized and rehydrated. After brief heating, the endogenous peroxidase activity was quenched, and sections were then incubated with the anti-RXR antibody (1:200 dilution). Sections were subsequently incubated with biotinylated goat anti-mouse antibody, then streptavidin-HRP

(Vectastain). Antigenic complexes were detected with 3,3′-diaminobenzidine, and sections were mounted in Mowiol (Kuraray). Images were collected with a Leica microscope and a camera coupled to the Leica IM500 image Manager software with ×10 magnification.

Primary antibodies used in Western blotting experiments were directed against RXRα (D-20, sc-553), RXRβ (C-20, sc-831), RXRγ (Y-20, sc-555), PPARγ (H-100, sc-7196; all from Santa Cruz Biotechnology Inc.), and UCH-L1 (3525S; Cell Signaling Technology). Secondary antibodies coupled to HRP were from Sigma-Aldrich. Immune complexes were detected using the ECL+ system from Amersham/GE Healthcare.

Yeast interaction assays. Yeast 2-hybrid experiments, as described by Carmona et al. (54), were carried out at Phenex GmbH.

ChIP assays. ChIP assays were carried out as described previously (58, 66). Primer sequences used in ChIP assays were described elsewhere (26), except for the Adpn promoter region (forward, 5′-CCATGCCTGCAGTCCATCTA-3′; reverse, 5′-GCTTCTGTCAAGCCATCCTGT-3′). The antibody to SMRT (PA1-844A) was from Affinity Bioreagents, whereas anti-NCoR (sc-1609), anti-PPARα (sc-9000), anti-PPARγ (sc-7196), anti-RXRα (sc-553), anti-RXRβ (sc-831), and anti-RXRγ (sc-555) were purchased from Santa Cruz Biotechnology Inc.

GST-pulldown assays. GST-pulldown experiments were performed as described previously (67). Data were acquired on a Storm 860 phosphorimager, and band intensities were quantified using ImageQuant TL software.

RNA extraction, Affymetrix analysis, and real-time PCR. Total RNA was prepared using the RNeasy minikit (Qiagen). Total RNA was isolated from mouse WAT or from 3T3-L1 cells using the RNAeasy Lipid Tissue kit (Qiagen). Purified RNA was adjusted to 1 g/l, and its integrity was assessed by gel electrophoresis or on an Agilent Bioanalyzer. RNA was purified from visWAT from 3 mice per group (OB/OB, OB/OB plus RSG, ob/ob, and ob/ob plus RSG) and hybridized to Affymetrix 430 2.0 arrays after cDNA labeling. Data were analyzed using the GeneSpring GX software (Agilent). Normalization was performed using the RMA algorithm, followed by a Benjamini-Hochberg false discovery rate statistical analysis. Genes that were significantly upregulated or repressed by more than 1.5-fold were then classified by a Gene Ontology functional classification. For RT-QPCR analysis of transcripts, reverse transcription was performed using random hexamers as recommended by the manufacturer (Promega). cDNAs were analyzed by PCR amplification using the TaqMan PCR master mix (Applied Biosystems) and a mix of actin primers and appropriate FAM probes. Absolute quantification of *RXR* mRNAs were determined by generating standard curves with known amounts of cloned RXR cDNAs. Actin, aP2, GyK, and Adpn primers and all other probes were purchased from Applied Biosystems (Assay on Demand). PCR (40 cycles) and data analysis were carried out using an ABI Prism 7500 (Perkin-Elmer).

RNA interference. Specific siRNA duplexes targeting RXRα, SMRT, and nonspecific siRNA controls were synthesized by Santa Cruz Biotechnology Inc. siRNAs were transfected using the DeliverX Plus siRNA transfection kit (Panomics) according to the manufacturer's guidelines.

Animal experiments. Mouse RNA and tissue samples were provided by M. Brun and A. Géant (Institut de Recherches Servier, Suresnes, France) and H. Duez (INSERM U545, Lille, France). OB/OB and ob/ob mice (8–10 weeks old) were purchased from Charles River. Mice were housed in a temperature-controlled room (22°C–24°C), with a relative humidity of 36%–80% and 12-hour light/dark cycles. Mice were fed ad libitum with free access to filtered tap water (0.22-μm filter) and received irradiated pelleted laboratory chow (A03-10; UAR) throughout the study, supplemented or not with RSG to achieve a 3-mg/kg/d intake. Mice were euthanized by cervical dislocation, and visWAT and scWAT were dissected, weighed, and immediately stored in liquid N_2. All procedures were validated by the ethical committee of the Institut Pasteur de Lille and carried out in accordance with European Union (EEC, no. 07430) and French ethical guidelines.

Isolation of stromal vascular fraction from WAT. Cells were prepared from WAT of obese or control mice as previously described (68), with minor modifications. Briefly, tissue was digested at 37°C in 1× PBS containing 0.2% BSA and 2 mg/ml collagenase (type II collagenase; Sigma-Aldrich). After filtration of the homogenate through 25-μm filters, mature adipocytes were separated from pellets (stromal vascular fraction) by centrifugation at 600 *g* for 10 minutes. After red cell lysis in 140 mM NH_4Cl and centrifugation, stromal vascular fraction cells were pelleted and resuspended in 1× PBS. Cells were seeded at 10,000 cells/cm² in DMEM-F12 supplemented with 10% newborn calf serum. Extensive washes were performed 12 hours later, and whole cell lysates were prepared 48 hours later.

Human tissues. Human tissue samples were provided by M.-F. Six and the Centre d'Investigations Cliniques (C.H.R.U. Lille). Human WAT samples were collected from patients undergoing abdominal surgery by laparoscopy or coeliosocopy after informed consent was obtained. All procedures were approved by the C.H.R.U. Lille ethical committee and were compliant to the French National Ethics Committee guidelines. Tissue samples from female patients — aged 35–59 years and not receiving any oral antidiabetic treatment — were removed within the first 30 minutes of the surgical procedure and immediately frozen in liquid N_2. Visceral fat was removed from the great omentum, and the subcutaneous fat was taken in the vicinity of the laparotomy incision. Based on biochemical and morphological parameters, patients were classified as lean (BMI, <25; fasting glucose [FG], 6 mM; oral glucose tolerance test [OGTT], <7.8 mM); obese (BMI, >35; FG, <6 mM; OGTT, <7.8 mM); obese glucose intolerant (BMI, >35; FG, between 6 and 7 mM, OGTT, between 7.8 and 11.1 mM) and obese diabetic (BMI, >35; FG, >7 mM; OGTT, >11.1 mM). Glycemia was assayed in the OGTT test 120 minutes after the glucose load.

Statistics. Data are mean ± SEM. Calculations were carried out using Prism software (GraphPAD Inc.). QPCR, Western blot, and transient transfection experiments were analyzed with the 2-tailed Student's *t* test. Statistical significance of differences between pairs of groups in animal studies was assessed using ANOVA followed by Tukey analysis. A *P* value less than 0.05 was considered significant.

Acknowledgments

The authors acknowledge the skillful technical assistance of M. André, B. Derudas, C. Brand, A. Lucas, and M. Ploton. We are indebted to M.-F. Six and the Centre d'Investigations Cliniques for human tissue samples; M. Brun, A. Géant, and H. Duez for mouse RNA and tissue samples; and J. Brozek (Genfit S.A.) for help with statistical analysis. This work was supported by research grants from Institut de Recherche Servier (IdRS), Région Nord-Pas de Calais/FEDER, and Fondation Coeur et Artères. A. Guédin, A. Langlois, B. Lefebvre, and Y. Benomar were supported by funds from IdRS.

Received for publication September 3, 2009, and accepted in revised form January 27, 2010.

Address correspondence to: Philippe Lefebvre, INSERM UMR 1011-Bâtiment J&K, Univ Lille-Nord de France, Faculté de Médecine de Lille-Pôle Recherche, Boulevard du Professeur Leclerc, 59045 Lille cedex, France. Phone: 33.3.20974220; Fax: 33.3.20974201; E-mail: philippe-claude.lefebvre@inserm.fr.

Bruno Lefebvre's present address is: INSERM U859, Faculté de Médecine de Lille-Pôle Recherche, Lille, France.

Luc Pénicaud's present address is: Centre des Sciences du Goût et de l'Alimentation, UMR 6265 CNRS, Dijon, France.

1. Montague CT, O'Rahilly S. The perils of portliness: causes and consequences of visceral adiposity. *Diabetes*. 2000;49(6):883–888.
2. Despres JP, et al. Abdominal obesity and the metabolic syndrome: contribution to global cardiometabolic risk. *Arterioscler Thromb Vasc Biol*. 2008;28(6):1039–1049.
3. Laplante M, et al. Mechanisms of the depot specificity of peroxisome proliferator-activated receptor gamma action on adipose tissue metabolism. *Diabetes*. 2006;55(10):2771–2778.
4. Lafontan M, Girard J. Impact of visceral adipose tissue on liver metabolism. Part I: heterogeneity of adipose tissue and functional properties of visceral adipose tissue. *Diabetes Metab*. 2008;34(4 Pt 1):317–327.
5. Goldberg RB. The new clinical trials with thiazolidinediones--DREAM, ADOPT, and CHICAGO: promises fulfilled? *Curr Opin Lipidol*. 2007; 18(4):435–442.
6. Heikkinen S, Auwerx J, Argmann CA. PPARgamma in human and mouse physiology. *Biochim Biophys Acta*. 2007;1771(8):999–1013.
7. Chao L, et al. Adipose tissue is required for the antidiabetic, but not for the hypolipidemic, effect of thiazolidinediones. *J Clin Invest*. 2000;106(10):1221–1228.
8. He W, et al. Adipose-specific peroxisome proliferator-activated receptor knockout causes insulin resistance in fat and liver but not in muscle. *Proc Natl Acad Sci U S A*. 2003;100(26):15712–15717.
9. Jones JR, et al. Deletion of PPAR in adipose tissues of mice protects against high fat diet-induced obesity and insulin resistance. *PNAS*. 2005;102(17):6207–6212.
10. Tontonoz P, Hu E, Graves RA, Budavari AI, Spiegelman BM. mPPAR gamma 2: Tissue-specific regulator of an adipocyte enhancer. *Genes Dev*. 1994;8(10):1224–1234.
11. Chawla A, Schwarz EJ, Dimaculangan DD, Lazar MA. Peroxisome proliferator-activated receptor (PPAR): Adipose- predominant expression and induction early in adipocyte differentiation. *Endocrinology*. 1994;135(2):798–800.
12. Lehmann JM, Moore LB, Smith-Oliver TA, Wilkison WO, Willson TM, Kliewer SA. An antidiabetic thiazolidinedione is a high affinity ligand for peroxisome proliferator-activated receptor gamma (PPAR). *J Biol Chem*. 1995;270(22):12953–12956.
13. Gray SL, Vidal-Puig AJ. Adipose tissue expandability in the maintenance of metabolic homeostasis. *Nutr Rev*. 2007;65(6 Pt 2):S7–12.
14. Choi KC, et al. Effect of PPAR-alpha and -gamma agonist on the expression of visfatin, adiponectin, and TNF-alpha in visceral fat of OLETF rats. *Biochem Biophys Res Commun*. 2005;336(3):747–753.
15. Laplante M, Sell H, MacNaul KL, Richard D, Berger JP, Deshaies Y. PPAR-gamma activation mediates adipose depot-specific effects on gene expression and lipoprotein lipase activity: mechanisms for modulation of postprandial lipemia and differential adipose accretion. *Diabetes*. 2003;52(2):291–299.
16. Yu JG, et al. The effect of thiazolidinediones on plasma adiponectin levels in normal, obese, and type 2 diabetic subjects. *Diabetes*. 2002;51(10):2968–2974.
17. Sanchez JC, et al. Effect of rosiglitazone on the differential expression of obesity and insulin resistance associated proteins in lep/lep mice. *Proteomics*. 2003;3(8):1500–1520.
18. Edvardsson U, Bergstrom M, Alexandersson M, Bamberg K, Ljung B, Dahllof B. Rosiglitazone (BRL49653), a PPARgamma-selective agonist, causes peroxisome proliferator-like liver effects in obese mice. *J Lipid Res*. 1999;40(7):1177–1184.
19. Metzger D, et al. Functional role of RXRs and PPARgamma in mature adipocytes. *Prostaglandins Leukot Essent Fatty Acids*. 2005;73(1):51–58.
20. Zhu Y, Qi C, Calandra C, Rao MS, Reddy JK. Cloning and identification of mouse steroid receptor coactivator-1 (mSRC-1), as a coactivator of peroxisome proliferator-activated receptor gamma. *Gene Expr*. 1996;6(3):185–195.
21. Gelman L, Zhou GC, Fajas L, Raspe E, Fruchart JC, Auwerx J. p300 interacts with the N- and C-terminal part of PPAR2 in a ligand-independent and -dependent manner, respectively. *J Biol Chem*. 1999;274(12):7681–7688.
22. Yuan CX, Ito M, Fondell JD, Fu ZY, Roeder RG. The TRAP220 component of a thyroid hormone receptor- associated protein (TRAP) coactivator complex interacts directly with nuclear receptors in a ligand-dependent fashion. *Proc Natl Acad Sci U S A*. 1998;95(14):7939–7944.
23. Puigserver P, Wu Z, Park CW, Graves R, Wright M, Spiegelman BM. A cold-inducible coactivator of nuclear receptors linked to adaptive thermogenesis. *Cell*. 1998;92(6):829–839.
24. Puigserver P, et al. Activation of PPARgamma coactivator-1 through transcription factor docking. *Science*. 1999;286(5443):1368–1371.
25. Yu C, Markan K, Temple KA, Deplewski D, Brady MJ, Cohen RN. The nuclear receptor corepressors NCoR and SMRT Decrease peroxisome proliferator-activated receptor transcriptional activity and repress 3T3-L1 adipogenesis. *J Biol Chem*. 2005;280(14):13600–13605.
26. Guan HP, Ishizuka T, Chui PC, Lehrke M, Lazar MA. Corepressors selectively control the transcriptional activity of PPAR in adipocytes. *Genes Dev*. 2005;19(4):453–461.
27. Nofsinger RR, et al. SMRT repression of nuclear receptors controls the adipogenic set point and metabolic homeostasis. *Proc Natl Acad Sci U S A*. 2008;105(50):20021–20026.
28. Glass CK, Rosenfeld MG. The coregulator exchange in transcriptional functions of nuclear receptors. *Genes Dev*. 2000;14(2):121–141.
29. Marfella R, et al. The possible role of the ubiquitin proteasome system in the development of atherosclerosis in diabetes. *Cardiovasc Diabetol*. 2007;6:35.
30. Paul S. Dysfunction of the ubiquitin-proteasome system in multiple disease conditions: therapeutic approaches. *Bioessays*. 2008;30(11-12):1172–1184.
31. Boudjelal M, Wang ZQ, Voorhees JJ, Fisher GJ. Ubiquitin/proteasome pathway regulates levels of retinoic acid receptor gamma and retinoid X receptor alpha in human keratinocytes. *Cancer Res*. 2000;60(8):2247–2252.
32. Pettersson F, et al. Rexinoids modulate SXR activity by increasing its protein turnover in a calpain-dependent manner. *J Biol Chem*. 2008;283(32):21945–21952.
33. Guenther MG, Barak O, Lazar MA. The SMRT and N-CoR corepressors are activating cofactors for histone deacetylase 3. *Mol Cell Biol*. 2001;21(18):6091–6101.
34. Gianni M, Tarrade A, Nigro EA, Garattini E, Rochette-Egly C. The AF-1 and AF-2 domains of RAR 2 and RXR Cooperate for triggering the transactivation and the degradation of RAR 2/RXR heterodimers. *J Biol Chem*. 2003;278(36):34458–34466.
35. Prufer K, Barsony J. Retinoid X receptor dominates the nuclear import and export of the unliganded vitamin d receptor. *Mol Endocrinol*. 2002;16(8):1738–1751.
36. Hershko A, Rose IA. Ubiquitin-aldehyde: a general inhibitor of ubiquitin-recycling processes. *Proc Natl Acad Sci U S A*. 1987;84(7):1829–1833.
37. Trayhurn P, Wang B, Wood IS. Hypoxia in adipose tissue: a basis for the dysregulation of tissue function in obesity? *Br J Nutr*. 2008;100(2):227–235.
38. Liu Y, et al. Discovery of inhibitors that elucidate the role of UCH-L1 activity in the H1299 lung cancer cell line. *Chem Biol*. 2003;10(9):837–846.
39. Orlicky DJ, DeGregori J, Schaack J. Construction of stable coxsackievirus and adenovirus receptor-expressing 3T3-L1 cells. *J Lipid Res*. 2001;42(6):910–915.
40. Direnzo J, et al. Peroxisome proliferator-activated receptors and retinoic acid receptors differentially control the interactions of retinoid X receptor heterodimers with ligands, coactivators, and corepressors. *Mol Cell Biol*. 1997;17(4):2166–2176.
41. el Jack AK, Hamm JK, Pilch PF, Farmer SR. Reconstitution of insulin-sensitive glucose transport in fibroblasts requires expression of both PPAR and C/EBP. *J Biol Chem*. 1999;274(12):7946–7951.
42. Duan SZ, et al. Hypotension, lipodystrophy, and insulin resistance in generalized PPAR-deficient mice rescued from embryonic lethality. *J Clin Invest*. 2007;117(3):812–822.
43. Setsuie R, Wada K. The functions of UCH-L1 and its relation to neurodegenerative diseases. *Neurochem Int*. 2007;51(2-4):105–111.
44. Takami Y, et al. Ubiquitin carboxyl-terminal hydrolase L1, a novel deubiquitinating enzyme in the vasculature, attenuates NF-kappaB activation. *Arterioscler Thromb Vasc Biol*. 2007;27(10):2184–2190.
45. Lopez-Avalos MD, Duvivier-Kali VF, Xu G, Bonner-Weir S, Sharma A, Weir GC. Evidence for a role of the ubiquitin-proteasome pathway in pancreatic islets. *Diabetes*. 2006;55(5):1223–1231.
46. Huss JM, Levy FH, Kelly DP. Hypoxia inhibits the peroxisome proliferator-activated receptor /retinoid X receptor gene regulatory pathway in cardiac myocytes: a mechanism for O2-dependent modulation of mitochondrial fatty acid oxidation. *J Biol Chem*. 2001;276(29):27605–27612.
47. Lavinsky RM, et al. Diverse signaling pathways modulate nuclear receptor recruitment of N- CoR and SMRT complexes. *Proc Natl Acad Sci U S A*. 1998;95(6):2920–2925.
48. Zamir I, Zhang J, Lazar MA. Stoichiometric and steric principles governing repression by nuclear hormone receptors. *Genes Dev*. 1997;11(7):835–846.
49. Allen T, et al. Halofenate is a selective peroxisome proliferator-activated receptor gamma modulator with antidiabetic activity. *Diabetes*. 2006;55(9):2523–2533.
50. Reginato MJ, et al. A potent antidiabetic thiazolidinedione with unique peroxisome proliferator-activated receptor gamma-activating properties. *J Biol Chem*. 1998;273(49):32679–32684.
51. Germain P, Iyer J, Zechel C, Gronemeyer H. Co-regulator recruitment and the mechanism of retinoic acid receptor synergy. *Nature*. 2002;415(6868):187–192.
52. Hauksdottir H, Farboud B, Privalsky ML. Retinoic acid receptors and do not repress, but instead activate target gene transcription in both the absence and presence of hormone ligand. *Mol Endocrinol*. 2003;17(3):373–385.
53. Farboud B, Privalsky ML. Retinoic acid receptor-alpha is stabilized in a repressive state by its C-terminal, isotype-specific F domain. *Mol Endocrinol*. 2004;18(12):2839–2853.
54. Carmona MC, et al. S 26948, a new specific PPAR modulator (SPPARM) with potent antidiabetic and antiatherogenic effects. *Diabetes*. 2007;55(9):2523–2533.
55. Burgermeister E, et al. A novel partial agonist of peroxisome proliferator-activated receptor-gamma (PPAR) recruits PPAR-coactivator-1alpha, prevents triglyceride accumulation, and potentiates insulin signaling in vitro. *Mol Endocrinol*. 2006;20(4):809–830.
56. Schupp M, et al. Molecular characterization of new selective peroxisome proliferator-activated receptor gamma modulators with angiotensin receptor blocking activity. *Diabetes*. 2005;54(12):3442–3452.
57. Gelman L, Feige JN, Desvergne B. Molecular basis of selective PPAR modulation for the treatment of Type 2 diabetes. *Biochim Biophys Acta*. 2007;1771(8):1094–1107.
58. Lefebvre B, Brand C, Flajollet S, Lefebvre P. Down-regulation of the tumor suppressor gene retinoic

acid receptor 2 through the phosphoinositide 3-Kinase/Akt signaling pathway. *Mol Endocrinol*. 2006;20(9):2109–2121.
59. Sacchetti P, Dwornik H, Formstecher P, Rachez C, Lefebvre P. Requirements for heterodimerization between the orphan nuclear receptor nurr1 and retinoid X receptors. *J Biol Chem*. 2002;277(38):35088–35096.
60. Duez H, et al. Regulation of human ApoA-I by gemfibrozil and fenofibrate through selective Peroxisome Proliferator-Activated Receptor modulation. *Arterioscler Thromb Vasc Biol*. 2005;25(3):585–591.
61. Depoix C, Delmotte MH, Formstecher P, Lefebvre P. Control of retinoic acid receptor heterodimerization by ligand-induced structural transitions. a novel mechanism of action for retinoid antagonists. *J Biol Chem*. 2001;276(12):9452–9459.
62. Forman BM. The antidiabetic agent LG100754 sensitizes cells to low concentrations of peroxisome proliferator-activated receptor gamma ligands. *J Biol Chem*. 2002;277(15):12503–12506.
63. Busch K, Martin B, Baniahmad A, Martial JA, Renkawitz R, Muller M. Silencing subdomains of v-ErbA interact cooperatively with corepressors: involvement of helices 5/6. *Mol Endocrinol*. 2000;14(2):201–211.
64. Musti AM, Treier M, Bohmann D. Reduced ubiquitin-dependent degradation of c-Jun after phosphorylation by MAP kinases. *Science*. 1997;275(5298):400–402.
65. Musti AM, Treier M, Peverali FA, Bohmann D. Differential regulation of c-Jun and JunD by ubiquitin-dependent protein degradation. *Biol Chem*. 1996;377(10):619–624.
66. Flajollet S, Lefebvre B, Rachez C, Lefebvre P. Distinct roles of the Steroid Receptor Coactivator 1 and of MED1 in retinoid-induced transcription and cellular differentiation. *J Biol Chem*. 2006;281(29):20338–20348.
67. Mouchon A, Delmotte M-H, Formstecher P, Lefebvre P. Allosteric regulation of the discriminative responsiveness of retinoic acid receptor to natural and synthetic ligands by retinoid X receptor and DNA. *Mol Cell Biol*. 1999;19(4):3073–3085.
68. Bjorntorp P, Karlsson M, Pertoft H, Pettersson P, Sjostrom L, Smith U. Isolation and characterization of cells from rat adipose tissue developing into adipocytes. *J Lipid Res*. 1978;19(3):316–324.